Chinese Chemical Letters 37 (2026) 112069

Contents lists available at ScienceDirect

Chinese Chemical Letters

journal homepage: www.elsevier.com/locate/cclet

Bioassay- and molecular network-guided discovery of PPAP derivatives from *Hypericum monogynum* with inhibitory activity against cardiac valve calcification

Bingchuan Geng[a,1], Jiangchun Wei[c,d,1], Dan Hu[a,1], Xingpiao Jin[d], Pingping Fan[b], Yahui Huang[b], Xiaoxuan Duan[c], Yipin Zhao[a,*], Yonghui Zhang[b,*], Zhengxi Hu[b,e,*]

[a] *Department of Cardiology, Heart Center of Henan Provincial People's Hospital, Central China Fuwai Hospital, Central China Fuwai Hospital of Zhengzhou University, Zhengzhou 450003, China*
[b] *Hubei Key Laboratory of Natural Medicinal Chemistry and Resource Evaluation, School of Pharmacy, Tongji Medical College, Huazhong University of Science and Technology, Wuhan 430030, China*
[c] *Laboratory of Clinical Research Center, Department of Pathology, Heping Hospital Affiliated to Changzhi Medical College, Changzhi 046000, China*
[d] *Shanxi Provincial Department-Municipal Key Laboratory Cultivation Base for Quality Enhancement and Utilization of Shang Dang Chinese Medicinal Materials, School of Pharmacy, Changzhi Medical College, Changzhi 046000, China*
[e] *Hubei Shizhen Laboratory, Wuhan 430061, China*

ARTICLE INFO

Article history:
Received 14 August 2025
Revised 3 November 2025
Accepted 5 November 2025
Available online 6 November 2025

Keywords:
Hypericum monogynum
PPAPs
Quantum chemical calculations
RNA sequencing
CAVD

ABSTRACT

Bioassay- and molecular network-guided isolation of the extract from *Hypericum monogynum* led to the identification of five polycyclic polyprenylated acylphloroglucinol (PPAP) derivatives, including a previously unreported bis-*seco* compound, hypermonane A (HMA, **1**). HMA possesses a unique 3/6-5/6/5 pentacyclic scaffold, characterized by C-1/C-2 and C-2/C-3 bond cleavage. In addition to HMA, four structurally related biosynthetic analogs (**2**–**5**) were also obtained. Its structure was elucidated using computer-assisted structure elucidation (CASE) software and gauge-independent atomic orbital (GIAO)-based nuclear magnetic resonance (NMR) calculations. The absolute configuration of **1** was determined through comparison of experimental and calculated electronic circular dichroism (ECD) spectra. Biological investigations revealed that HMA potently inhibited aortic valve calcification by simultaneously suppressing osteogenic differentiation (runt-related transcription factor 2/alkaline phosphatase, RUNX2/ALP) and extracellular matrix remodeling (collagen type I alpha 1 chain/a disintegrin and metalloproteinase with thrombospondin motif 4, COL1A1/ADAMTS4). Moreover, in a murine model of calcific aortic valve disease (CAVD), HMA significantly attenuated pathological aortic valve calcification. These findings highlight HMA as a promising lead compound for the development of anti-CAVD therapeutics.

© 2026 Published by Elsevier B.V. on behalf of Chinese Chemical Society and Institute of Materia Medica, Chinese Academy of Medical Sciences.

Calcific aortic valve disease (CAVD) is a highly prevalent valvular disorder and represents the third leading cause of cardiovascular morbidity worldwide [1,2]. It affects approximately 2 % of individuals over the age of 70, contributing to an estimated 12.6 million cases annually on a global scale [3,4]. The pathogenesis of CAVD involves a multifactorial and progressive process, characterized by complex interactions among valvular endothelial cells, interstitial cells, and immune cells, ultimately driving structural remodeling of the aortic valve leaflets and disease progression [5,6]. Despite extensive clinical and basic research efforts, the underlying molecular mechanisms initiating and advancing CAVD remain incompletely understood. As a result, no pharmacological therapy has been approved to prevent or halt its progression, and surgical aortic valve replacement continues to be the only effective intervention currently available [5,7,8]. These limitations underscore the urgent need for the development of novel therapeutic agents with the capacity to attenuate or reverse valvular calcification.

As part of our ongoing investigation into bioactive natural products from *Hypericum* species [9–11], we employed a combined strategy integrating bioactivity-guided screening and molecular networking to explore *H. monogynum*, which led to the isolation of hypermonane A (HMA, **1**), a structurally unique bis-*seco* polycyclic polyprenylated acylphloroglucinol (PPAP) bearing an unprecedented 3/6-5/6/5 pentacyclic scaffold, along with four known biosynthetic analogs (**2**–**5**). Herein, we reported the iso-

* Corresponding authors.
E-mail addresses: zhao1pin@gmail.com (Y. Zhao), zhangyh@mails.tjmu.edu.cn (Y. Zhang), hzx616@126.com (Z. Hu).
[1] These authors contributed equally to this work.

https://doi.org/10.1016/j.cclet.2025.112069
1001-8417/© 2026 Published by Elsevier B.V. on behalf of Chinese Chemical Society and Institute of Materia Medica, Chinese Academy of Medical Sciences.

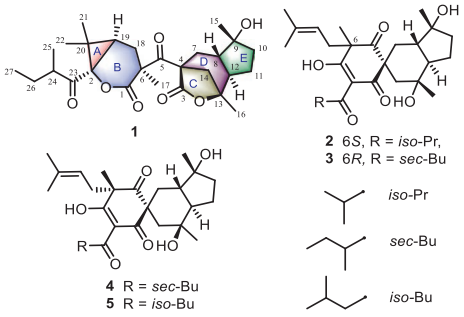


Fig. 1. Chemical structures of compounds **1**–**5**.

lation, structural elucidation, and bioactivity evaluation of these compounds (Fig. 1).

The residual 95% ethanol extract of *H. monogynum* was suspended in water and subsequently partitioned with petroleum ether (PE). Silica gel column chromatography of the PE extract afforded six main fractions (Fr. A–Fr. F). To investigate potential anti-calcific activity, we first examined the expression of runt-related transcription factor 2 (RUNX2), a key osteogenic transcription factor, in human aortic valve tissues. Western blot (WB) analysis showed a marked upregulation of RUNX2 in CAVD samples compared to healthy controls (healthy: $n = 18$; CAVD: $n = 24$) (Figs. 2A and B). Aortic valve samples in the control group were obtained from patients with dilated cardiomyopathy undergoing heart transplantation, with echocardiography confirming absence of calcification. In the calcification group, samples were collected from patients undergoing aortic valve replacement for calcific aortic valve disease (CAVD); exclusion criteria comprised rheumatic heart disease, infective endocarditis, or bicuspid aortic valve. Additionally, time-dependent elevation of RUNX2 expression was observed in human valvular interstitial cells (hVICs) treated with osteogenic medium (OM) (Figs. 2C and D), indicating successful induction of the calcification phenotype. Using our in-house developed high-throughput screening platform, we assessed the anti-calcific potential of each fraction by monitoring RUNX2 protein levels in OM-treated hVICs [11–16]. Among all fractions, Fr. E exhibited the most significant inhibitory activity and was thus selected for further separation, yielding seven subfractions (Fr. E1–Fr. E7). Subsequent evaluation of these subfractions using the same screening strategy revealed that Fr. E6 showed the strongest inhibitory effect on OM-induced calcification (Fig. 2E). Bioactivity-guided isolation from Fr. E6 ultimately led to the identification of five PPAPs, including one previously undescribed compound (**1**) bearing a novel 3/6-5/6/5 pentacyclic scaffold, along with four known biosynthetic analogs (**2**–**5**). The molecular networking cluster containing the above compounds was expanded, with nodes labeled according to their parent *m*/*z* values (Figs. 2F and G).

HMA (**1**) possessed the molecular formula $C_{27}H_{38}O_7$, as determined by the ^{13}C nuclear magnetic resonance (NMR) and high-resolution electrospray ionization mass spectrometry (HRESIMS) data (*m*/*z* 497.2508, $[M+Na]^+$, calcd. for $C_{27}H_{38}O_7Na^+$, 497.2515), indicating nine degrees of unsaturation. The ^1H NMR spectrum (Table S1 in Supporting information) exhibited resonances for one *sec*-butyl group (δ_H 3.11, m; 1.08, d, $J = 7.2$ Hz; 1.72, m; 1.34, m; 0.85, t, $J = 7.2$ Hz) and five methyl singlets. The ^{13}C and distor-

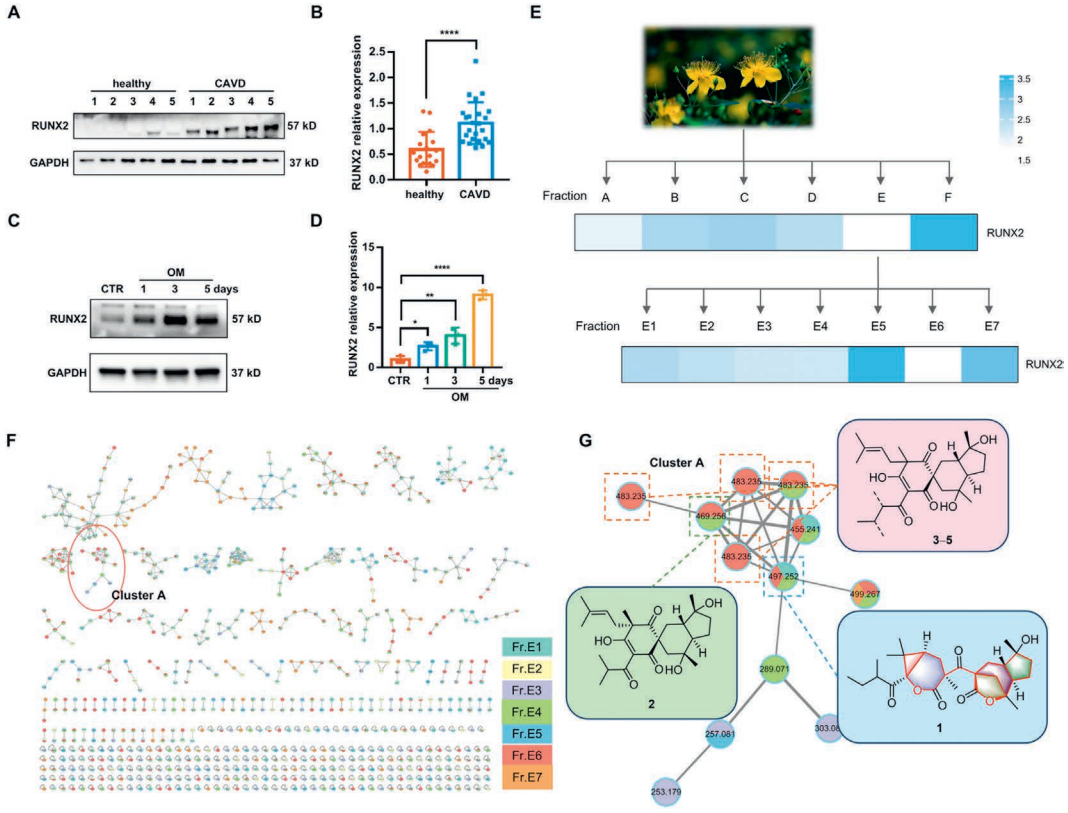
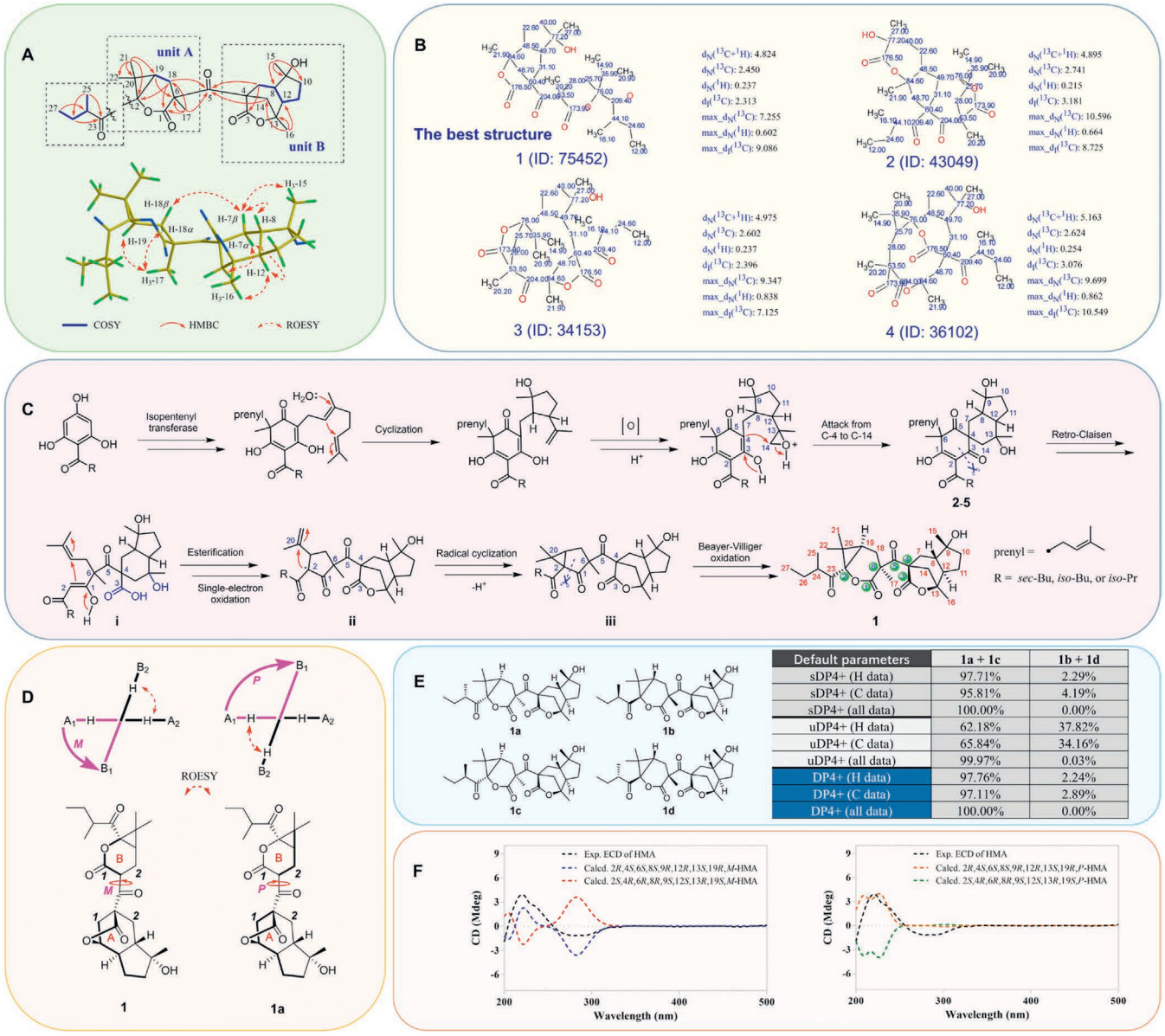


Fig. 2. Establishment of a bioassay- and molecular network-guided discovery strategy. (A, B) WB analysis of RUNX2 protein expression in human aortic valve tissues from CAVD patients *vs.* healthy controls. (C, D) Time-dependent upregulation of RUNX2 in OM-induced hVICs following treatment for 1, 3, or 5 days. CTR: control; GAPDH: glyceraldehyde-3-phosphate dehydrogenase. $^*P < 0.05$, $^{**}P < 0.01$, $^{****}P < 0.0001$ ($n = 3$). (E) Workflow of the bioassay-guided isolation strategy from *H. monogynum* extract. (F) Tandem mass spectrometry (MS/MS)-based molecular network generated from the extract fractions of *H. monogynum*, showing the expanded cluster of protonated ions. (G) Detailed molecular network highlighting compounds **1**–**5**. Each node is represented by a pie chart, where the colored segments indicate the relative spectral contributions from each sample group. Data are presented as mean ± standard deviation (SD).



Default parameters	1a + 1c	1b + 1d
sDP4+ (H data)	97.71%	2.29%
sDP4+ (C data)	95.81%	4.19%
sDP4+ (all data)	100.00%	0.00%
uDP4+ (H data)	62.18%	37.82%
uDP4+ (C data)	65.84%	34.16%
uDP4+ (all data)	99.97%	0.03%
DP4+ (H data)	97.76%	2.24%
DP4+ (C data)	97.11%	2.89%
DP4+ (all data)	100.00%	0.00%

Fig. 3. Multi-technique structural elucidation of **1**. (A) Key ^{1}H–^{1}H COSY, HMBC, and ROESY correlations observed for **1**. (B) Optimal planar structures of **1** proposed by the ACD/structure elucidator suite. (C) Proposed biosynthetic pathway of **1**. (D) Diagnostic ROESY correlations for HMA (2*R*,4*S*,6*S*,8*S*,9*R*,12*R*,13*S*,19*R*,*M*) (**1**) and the atropisomeric molecule (**1a**) (2*R*,4*S*,6*S*,8*S*,9*R*,12*R*,13*S*,19*R*,*P*). (E) Statistical analysis of DP4+ parameters for **1**. (F) Experimental ECD spectrum of HMA (**1**) (black) and the calculated ECD spectra for 2*R*,4*S*,6*S*,8*S*,9*R*,12*R*,13*S*,19*R*,*M*-**1** (blue), 2*S*,4*R*,6*R*,8*R*,9*S*,12*S*,13*R*,19*S*,*M*-**1** (red), 2*R*,4*S*,6*S*,8*S*,9*R*,12*R*,13*S*,19*R*,*P*-**1** (orange), and 2*S*,4*R*,6*R*,8*R*,9*S*,12*S*,13*R*,19*S*,*P*-**1** (green).

tionless enhancement by polarization transfer (DEPT) NMR (Table S1) spectra showed 27 carbon resonances including seven methyls, six methylenes, four methines, and ten quaternary carbons. Comprehensive 2D NMR analysis revealed that HMA belonged to a PPAP derivative, comprising two characteristic structural units (units A and B, Fig. 3A). The proton-proton correlation spectroscopy (^{1}H–^{1}H COSY) spectrum revealed three independent spin systems: H_3-25/H-24/H_2-26/H_3-27, H_2-18/H-19, and H_2-7/H-8/H-12/H_2-11/H_2-10 (Fig. 3A). Structural elucidation of unit A was achieved through key heteronuclear multiple bond correlation (HMBC) correlations from H_3-17 to C-1/C-6/C-18, from H_3-21/H_3-22 to C-2/C-19, from H-19 to C-6, and from H_2-18 to C-1/C-2 (Fig. 3A). Similarly, unit B was characterized by the HMBC correlations from H_3-15 to C-8/C-9/C-10 and from H_3-16 to C-12/C-13/C-14. Critical inter-unit connectivity was established *via* the HMBC correlations from H_3-17 (unit A), H_2-7 (unit B), and H_2-14 (unit B) to the carbonyl carbon (C-5). The precise connectivity of the 2-methylbutyryl group with structural fragments A and B could not be unambiguously determined due to the absence of key correlation signals in NMR data. However, based on (1) C-2 being the sole remaining unsubstituted position in the molecular framework and (2) the well-documented prevalence of 2-methylbutyryl substitution at C-2 in PPAPs, we provisionally assigned this acyl group to C-2 of unit A. The planar structure of compound **1** was definitively confirmed by computational analysis using advanced chemistry development (ACD)/structure elucidator (Fig. 3B) [17–19], and the proposed biosynthetic pathway further supported the rationality (Fig. 3C).

The relative configuration of **1** was elucidated through detailed analysis of its rotating-frame overhauser effect spectroscopy (ROESY) data (Fig. 3A). A key correlation between H-19 and H_3-17 suggested their spatial proximity on the same molecular face, which was tentatively assigned as α-oriented. This stereochemical assignment further indicated that the C-2 isovaleryl group and

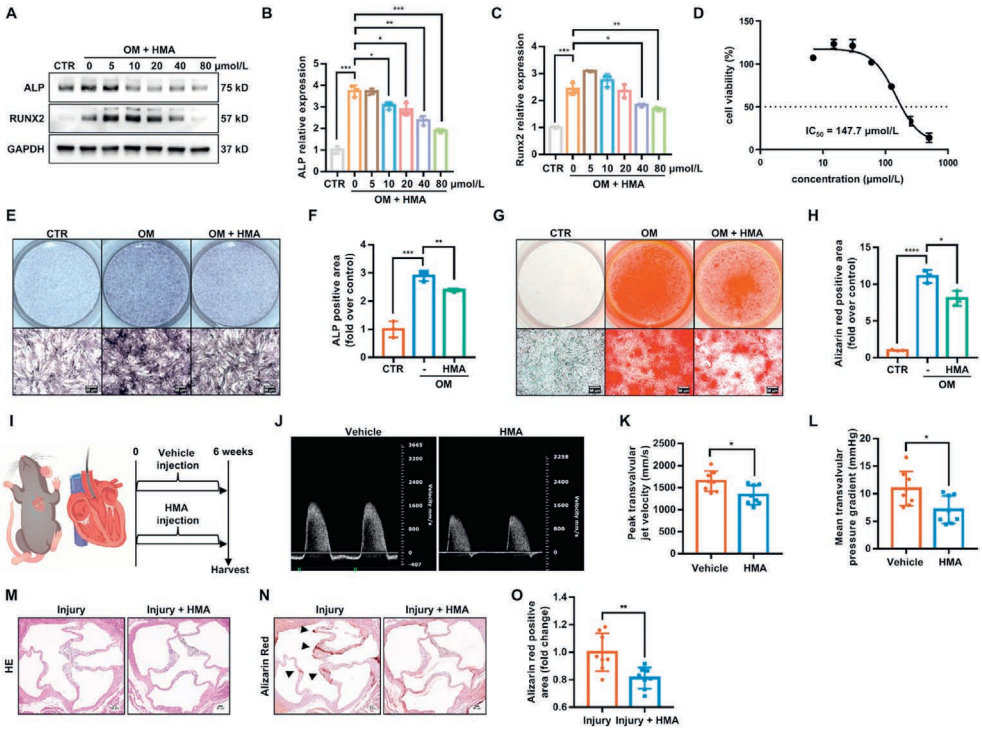


Fig. 4. Compound HMA mitigated VIC calcification in *in vitro* and *in vivo* models. (A–C) WB analysis of RUNX2 and ALP protein levels in hVICs cultured in OM and treated with increasing concentrations of compound HMA ($n = 3$). (D) Cell viability assay (CCK-8) showing IC_{50} value (147.7 μmol/L) after 72 h HMA exposure. (E, F) ALP activity staining and quantitative analysis in CTR, OM, and OM+HMA (40 μmol/L) groups ($n = 3$). (G, H) Mineralization assessed by Alizarin Red staining and quantification in CTR, OM, and OM+HMA (40 μmol/L) groups ($n = 3$). (I) Workflow diagram for animal experiments. (J) Representative echocardiograms 6 weeks post-injury. (K, L) HMA treatment (20 mg/kg per 3 days, i.p.) reduces peak transvalvular jet velocity (K) and mean transvalvular pressure gradient (L) ($n = 8$). (M–O) HE staining (M) and Alizarin Red staining (N) showing significantly reduced calcium accumulation in aortic valve of HMA-treated mice ($n = 8$). Scale bar: 50 μm. Data were analyzed using *t*-test and presented as mean ± SD. $^{*}P < 0.05$, $^{**}P < 0.01$, $^{***}P < 0.001$, $^{****}P < 0.0001$.

the cyclopropyl moiety were α- and β-oriented, respectively. Additional ROESY correlations of H-8/H-7β, H-7β/H_3-15, H-12/H-7α, and H-12/H_3-16 established that H-8 and H_3-15 resided on the same molecular face, whereas H-12 and H_3-16 were located on the opposite face.

Due to restricted rotation around the bond adjacent to the C-6 carbonyl and the absence of detectable NMR signals for multiple conformers, compound **1** was deduced to exist as an atropisomer [20,21]. Structural modeling of two possible atropisomeric forms (**1** and **1a**) revealed that only the 2*R**,4*S**,6*S**,8*S**,9*R**,12*R**,13*S**,19*R**,*M* configuration of **1** was consistent with the observed ROESY cross-peaks, especially the spatial proximity between H-7β and H-18β (Fig. 3D). To further validate the relative stereochemistry, ^{13}C NMR chemical shifts for four candidate diastereomers (**1a**–**1d**) were computed using the Gauge-independent atomic orbital (GIAO) method. The calculated shifts were statistically analyzed and compared with experimental data *via* the DP4+ method (Fig. 3E and Fig. S1 in Supporting information), supporting the proposed configuration [22]. The absolute configuration of **1** was subsequently confirmed by time-dependent density functional theory (TDDFT)-based electronic circular dichroism (ECD) calculations, which showed excellent agreement between the experimental and calculated curves (Fig. 3F).

According to the previous reports, the known compounds were identified as chipericumin C (**2**) [23], chipericumin D (**3**) [23], monosescinol B (**4**) [24], and monosescinol C (**5**) [24].

Further investigations revealed that compound **1** (HMA) significantly downregulated the expression of osteogenic markers RUNX2 and alkaline phosphatase (ALP) and alleviated calcification in hVICs. Under OM conditions, escalating HMA concentrations (5–80 μmol/L) modulated RUNX2 and ALP expression (Figs. 4A–C). The half maximal inhibitory concentration (IC_{50}) value of HMA against hVICs was determined to be 147.7 μmol/L *via* cell counting kit-8 (CCK-8) viability assays (Fig. 4D). During extended osteogenic culture, HMA also exerted anti-calcific effects. ALP activity assays revealed significantly reduced enzymatic activity in HMA-treated hVICs after 7-day OM culture (Figs. 4E and F). Alizarin Red staining confirmed attenuated calcium deposition in HMA-treated cultures following 21-day osteogenic induction (Figs. 4G and H).

To elucidate the underlying mechanisms by which compound HMA alleviates calcification in hVICs, we performed network pharmacology analysis (Figs. 5A and B) and RNA sequencing (Fig. 5C). Utilizing the Comparative Toxicogenomics Database (CTD) and GeneCards databases, 76 HMA-related target genes and 534 CAVD-related target genes were identified by identifying intersections (Fig. 5A). Further cross-referencing of these two datasets revealed 65 overlapping target genes (Fig. 5B). Transcriptomic profiling of hVICs under OM induction demonstrated profound dysregulation of calcification related signal pathways. Volcano plots identified key differentially expressed genes (DEGs), including actin, alpha 2, smooth muscle (ACTA2) (upregulated in OM *vs.* CTR; downregulated in OM+HMA *vs.* OM) (Figs. 5D and E). Comparative analysis of upregulated genes highlighted HMA-specific suppression of extracellular matrix (ECM)-remodeling (collagen type I alpha 1 chain, COL1A1; a disintegrin and metalloproteinase with thrombospondin motif 4, ADAMTS4) and osteogenic (alkaline phosphatase, ALP; twist-related protein 2, TWIST2) targets (Figs. 5F and G). Functional enrichment analysis (Figs. 5H and I) further confirmed HMA's role in counteracting CAVD progression, with significant inhibition of biological processes critical to calcification: ECM organization, cellular response to stress, and sulfur compound metabolism. As validated by quantitative polymerase chain reaction (qPCR), HMA

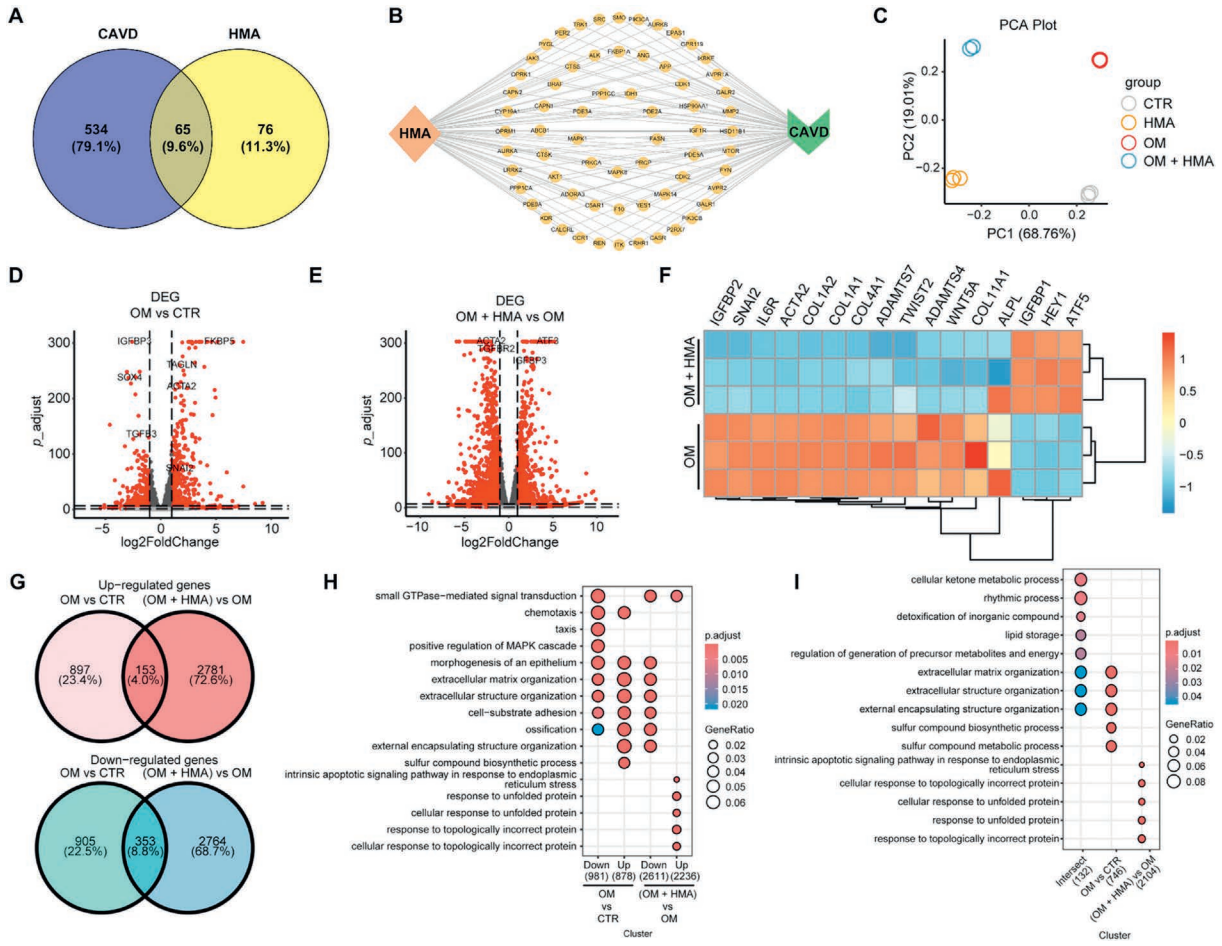


Fig. 5. Network pharmacology and transcriptomic analysis of OM-induced aortic valve calcification and the effect of HMA treatment. (A) The Venn diagram of targets number of HMA and CAVD. (B) The HMA-CAVD target network. (C) Principal component analysis (PCA) plot displaying the transcriptomic profiles of four groups. (D, E) Volcano plot of DEGs in OM *vs.* CTR and OM+HMA *vs.* OM (thresholds: $|\log2FC| > 0.6$, adjusted $P < 0.05$). (F) Heatmap of gene expression profiles associated with aortic valve calcification in OM and OM+HMA groups, demonstrating the regulatory effect of HMA on calcification-related genes. (G) Venn diagram illustrating the overlap of up- and down-regulated DEGs between OM *vs.* CTR and OM+HMA *vs.* OM comparisons. (H) Dot plot of gene ontology biological process (GOBP) enrichment analysis for up- and down-regulated DEGs from panels D and E. Dot size represents gene count; color indicates adjusted *P*-value. (I) Dot plot of GOBP enrichment for the intersecting up-regulated DEGs identified in panel G, revealing key biological processes affected by OM and reversed by HMA. FC: fold change.

treatment significantly downregulated the mRNA expression levels of key calcification-related genes, including ADAMTS4, TWIST2, and COL1A1, in hVICs under osteogenic conditions (Figs. S2A–C in Supporting information). Furthermore, molecular docking analysis revealed strong binding affinities between HMA and the core transcription factors RUNX2 and TWIST2, with favorable docking scores of −6.6 and −6.9 kcal/mol, respectively (Figs. S2D and E in Supporting Information), suggesting a potential direct mechanism for its inhibitory action.

The wire injury model rapidly recapitulates the core pathological features of CAVD, characterized by sequential inflammation, fibrosis, and calcification, through controlled mechanical damage. This model provides a robust platform to investigate molecular mechanisms and therapeutic windows for phytomedicine components targeting aortic valve calcification [13,15]. To determine whether HMA administration ameliorates CAVD progression *in vivo*, we established a wire injury-induced murine CAVD model and randomized animals into two cohorts: HMA-treated group: Intraperitoneal injections of HMA (20 mg/kg) every 72 h for 6 weeks ($n = 8$); Vehicle control group: Equivalent volumes of saline administered on identical schedule ($n = 8$). The Animal Care and Use Committee of the Wuhan Food and Drug Safety Evaluation Center sanctioned all animal studies (approval No. 202410342). Post-treatment assessments included echocardiography for cardiac function and histomorphometry for valvular calcification quantification (Fig. 4I). HMA-treated mice exhibited significant functional improvements *vs.* vehicle controls, with pronounced reductions in hemodynamic parameters (peak transvalvular pressure gradients; mean pressure gradients, Figs. 4J–L). Pathological calcification was significantly attenuated in HMA-treated aortic valves, as evidenced by Alizarin Red staining (Figs. 4M–O). Collectively, these data demonstrate that HMA attenuates CAVD progression by mitigating hemodynamic impairment and pathological calcification, highlighting its therapeutic potential.

In conclusion, by employing a bioassay- and molecular network-guided discovery strategy, HMA, a novel C-1/C-2, C-2/C-3 bis-*seco* PPAP derivative with a unique 3/6-5/6/5 pentacyclic scaffold, was identified from *H. monogynum*. Its absolute configuration was unequivocally established through an integrated approach combining computer-assisted structure elucidation (CASE) and GIAO-based NMR and ECD calculations. HMA exhibited potent anti-calcific activity in CAVD model, acting *via* dual inhibition of osteogenic differentiation (RUNX2/ALP) and extracellular matrix remodeling (COL1A1/ADAMTS4). *In vivo* studies using a wire injury-induced CAVD mouse model further validated its efficacy, demonstrating significant attenuation of valvular calcification. Structurally, the distinctive double-ring-opening of the phloroglucinol core appears pivotal to its bioactivity, as the precursor spiro-

cyclic PPAP analogs showed negligible anti-calcific effects. This indicates that the formation of new core ring systems following ring-opening, particularly the generation of two lactone rings, plays a critical role in mediating anti-calcific activity. The lactone moieties in the structure are crucial for the drug molecule to exert its key biological activity and are recognized as essential pharmacophoric groups.

To position HMA within the current therapeutic landscape, we compared its mechanism with clinical-stage strategies. Unlike bisphosphonates, which primarily inhibit hydroxyapatite deposition, or NOTCH-pathway targeted agents focusing on a specific signaling axis, HMA offers a distinct dual-inhibitory advantage by concurrently suppressing both osteogenic differentiation and pathological ECM remodeling. This multifaceted action, targeting two key drivers of CAVD progression, may translate into a more comprehensive therapeutic effect for slowing disease advancement. Therefore, HMA presents a novel and promising lead compound for developing multi-target therapies against CAVD. These findings position HMA as a promising first-in-class small-molecule inhibitor for CAVD, addressing a critical unmet need for pharmacological intervention beyond surgical valve replacement. Future studies will focus on optimizing its pharmacokinetic properties and evaluating potential synergistic effects with anti-inflammatory agents.

CRediT authorship contribution statement

Bingchuan Geng: Writing – review & editing, Writing – original draft, Methodology. **Jiangchun Wei:** Writing – review & editing, Writing – original draft, Formal analysis, Data curation. **Dan Hu:** Writing – review & editing, Writing – original draft, Methodology, Formal analysis. **Xingpiao Jin:** Software, Data curation, Conceptualization. **Pingping Fan:** Software, Formal analysis, Data curation. **Yahui Huang:** Visualization, Software, Formal analysis. **Xiaoxuan Duan:** Software, Formal analysis, Data curation, Conceptualization. **Yipin Zhao:** Supervision, Resources, Investigation. **Yonghui Zhang:** Visualization, Software, Formal analysis, Data curation. **Zhengxi Hu:** Validation, Supervision, Resources.

Ethical statement

The Review Board of Central China Fuwai Hospital authorized all human experiments (approval No. 202576). Informed consent was obtained from all participants, and the study complied with the Declaration of Helsinki.

Declaration of competing interest

The authors declare that they have no known competing financial interests or personal relationships that could have appeared to influence the work reported in this paper.

Acknowledgments

We thank the Analytical and Testing Center at Huazhong University of Science and Technology (HUST) for measuring HRESIMS, ECD, UV, and IR data. Thanks also for the Medical Subcenter of HUST Analytical & Testing Center for measuring NMR data. This work was supported by the National Natural Science Foundation of China (Nos. 82273811, 22577033, 82470380, and 82404822), the National Program for Support of Top-notch Young Professionals (No. 0106514050), the China Postdoctoral Science Foundation (No. 2023M742415), the Hubei Provincial Natural Science Foundation of China (No. 2024AFA028), the Scientific and Technological Innovation Programs of Higher Education Institutions in Shanxi (No. 2025Q030), the National Key Research and Development Program of China (No. 2021YFA0910500), the Fundamental Research Funds for the Central Universities (No. 2025BRA015), the Guangdong Basic and Applied Basic Research Foundation (No. 2023A1515110763), and the Henan Provincial Medical Science and Technology Key Program (No. LHGJ20240152).

Supplementary materials

Supplementary material associated with this article can be found, in the online version, at doi:10.1016/j.cclet.2025.112069.

References

[1] G. Artiach, M. Carracedo, O. Plunde, et al., Circulation 142 (2020) 776–789.
[2] S. Sánchez-Esteban, M. Castro-Pinto, A. Cook-Calvete, et al., Antioxidants 11 (2022) 1736.
[3] U. Majumdar, S. Manivannan, M. Basu, et al., Sci. Adv. 7 (2021) eabe3706.
[4] P. Généreux, P. Pibarot, B. Redfors, et al., Eur. Heart J. 38 (2017) 3351–3358.
[5] Moncla.Louis-Hippolyte Minvielle, B. Mewen, B. Yohan, M. Patrick, Nat. Rev. Cardiol. 20 (2023) 546–559.
[6] E. The, D.M. de Graaf, Y. Zhai, et al., Proc. Natl. Acad. Sci. U. S. A. 119 (2022) e2202577119.
[7] Y. Wang, Y. Fang, P. Lu, et al., Front. Cardiovasc. Med. 8 (2021) 682298.
[8] L. Lop, A.H. Chester, R.O. Sampaio, et al., Front. Cardiovasc. Med. 9 (2022) 998862.
[9] J. Wei, P. Fan, X. Jin, et al., Org. Chem. Front. 11 (2024) 5350–5357.
[10] J. Wei, P. Fan, Y. Huang, et al., Org. Chem. Front. 11 (2024) 3459–3464.
[11] T. Zhang, J. Wei, X. Jin, et al., Phytochem. Lett. 65 (2025) 77–81.
[12] C. Jiang, D. Yao, Z. Liu, et al., Redox Biol. 73 (2024) 103215.
[13] B. Geng, X. Chen, J. Chi, et al., Theranostics 13 (2023) 3781–3793.
[14] Y. Huang, C. Wang, T. Zhou, et al., Eur. Heart J. 45 (2024) ehae407.
[15] Z. Liu, K. Wang, C. Jiang, et al., Adv. Sci. 11 (2024) 2307319.
[16] Z. Liu, N. Dong, H. Hui, et al., Eur. Heart J. 43 (2022) 1652–1664.
[17] C.M. Sai, N.B. Qin, C.C. Jia, et al., Chin. Chem. Lett. 27 (2016) 1717–1720.
[18] D. Chen, J. Li, X. Xu, et al., Chin. Chem. Lett. 35 (2024) 109451.
[19] Z. Guo, P. Ji, S. Yang, et al., Org. Chem. Front. 12 (2025) 3750–3758.
[20] E. Gougoula, J. Pfeiffer, M. Schnell, F. Tambornino, Phys. Chem. Chem. Phys. 26 (2024) 25678–25687.
[21] D.L.M. Vasconcelos, C.B. Silva, A.M.R. Teixeira, P.T.C. Freire, et al., J. Mol. Struct. 1243 (2021) 130872.
[22] Q. Lin, H. Xie, Q. Tang, et al., Org. Lett. 27 (2025) 3273–3278.
[23] S. Abe, N. Tanaka, J. Kobayashi, J. Nat. Prod. 75 (2012) 484–488.
[24] Z. Shi, J. Yin, Y. Xiao, et al., Chin. Chem. Lett. 35 (2024) 109458.